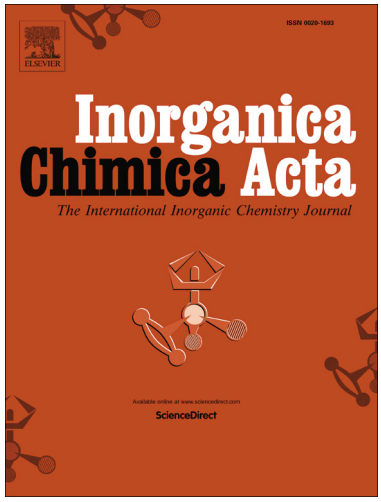

Research paper

Two Heptacoordinated Manganese(II) complexes of giant pentadentate *s*-triazine *bis*-Schiff base ligand: Synthesis, crystal structure, biological and DFT studies

Saied M. Soliman, Ayman El-Faham, Sobhy E. Elsilk, Muhammad Farooq

PII: S0020-1693(18)30331-1
DOI: https://doi.org/10.1016/j.ica.2018.04.043
Reference: ICA 18234

To appear in: *Inorganica Chimica Acta*

Received Date: 2 March 2018
Revised Date: 19 April 2018
Accepted Date: 22 April 2018

Please cite this article as: S.M. Soliman, A. El-Faham, S.E. Elsilk, M. Farooq, Two Heptacoordinated Manganese(II) complexes of giant pentadentate *s*-triazine *bis*-Schiff base ligand: Synthesis, crystal structure, biological and DFT studies, *Inorganica Chimica Acta* (2018), doi: https://doi.org/10.1016/j.ica.2018.04.043

Two Heptacoordinated Manganese(II) complexes of giant pentadentate *s*-triazine *bis*-Schiff base ligand: Synthesis, crystal structure, biological and DFT studies

Saied M. Soliman[a,c]*, Ayman El-Faham[b,c], Sobhy E. Elsilk[a,d], Muhammad Farooq[f]

[a]Department of Chemistry, Rabigh College of Science and Art, King Abdulaziz University, P.O. Box 344, Rabigh 21911, Saudi Arabia, Email: saied1soliman@yahoo.com.

[b]Department of Chemistry, College of Science, King Saud University, P. O. Box 2455, Riyadh 11451, Saudi Arabia, Email: aymanel_faham@hotmail.com

[c]Department of Chemistry, Faculty of Science, Alexandria University, P.O. Box 426, Ibrahimia, Alexandria 21321, Egypt; Email: saied1soliman@yahoo.com.

[d]Bacteriology Unit, Botany Department, Faculty of Science, Tanta University, Tanta 31527, Egypt, Email: selsilk@yahoo.de.

[f]Department of Zoology, Bioproducts Research Chair, College of Science, King Saud University, P.O. Box 2455, Riyadh 11451, Saudi Arabia, Email: fmuhammad@ksu.edu.sa

Abstract

A new *s*-triazine *bis*-Schiff base chelating ligand (**L**) and two of its heptacoordinated Mn(II) complexes were synthesized and characterized. Reaction of solid $Mn(NO_3)_2.4H_2O$ with methanolic solution of the ligand (**L**; **5)** afford $[MnL(MeOH)NO_3]NO_3.MeOH$; (**6**). While, repeating the reaction in water/methanol solution, the complex $[MnL(H_2O)_2](NO_3)_2$; **7** was formed. In both complexes, the Mn(II) is coordinated with **L** as a pentadentate ligand *via* its N-atoms augmented with two axial Mn-O bonds leading to a distorted pentagonal bipyramidal configuration around the Mn(II) ion. The two-pyridine moieties at the end of the ligand arms are twisted from one another due to the short contact distance between the two hydrogen atoms at the 6 position of the pyridine moieties. As a result, the strength of the Mn-N bonds decrease ongoing from the triazine moiety towards the outside of the ligand arms. The atoms in molecules topological parameters correlated well with the Mn-N distances. The Mn-N and Mn-O bonds were analyzed using natural bond orbital calculations. Both complexes showed higher thermal stability than the free ligand. Antimicrobial studies showed that **7** and **L** are the best candidates as antifungal and antibacterial agents, respectively. The mechanism of biological activity depends on the interactions between the compound and cell wall.

Keywords: Manganese(II); *s*-triazine Schiff base; heptacoordinated; antimicrobial; K^+ leakage

1. Introduction

Triazine compounds are important class of ligands in coordination chemistry [1] and for molecular encapsulation [2]. These derivatives are important heterocyclic compounds with interesting biological, pharmaceutical [3–10] and, and industrial applications [11]. Also, these nitrogen-rich molecules have potential use as energetic explosives [12] and organic corrosion inhibitors [13]. An important advantage of the *s*-triazine derivatives is the ease of their preparation from the cheap cyanuric chloride (CC; $C_3N_3Cl_3$). The chlorine atoms in the cyanuric chloride molecule could be simply substituted by different nucleophiles and depending on the reaction condition, such as temperature, various mono, di- and tri-substituted *s*-triazine derivatives [14–19] could be obtained. In this regard, cyanuric chloride can react with hydrazine hydrate smoothly under reflux or ultrasonic irradiation to afford the mono-, di- or tri-substituted hydrazino-derivatives in almost quantitative yield [20]. The *s*-triazine building blocks are important ligands in supramolecular chemistry [21] due to their ability to make π-π stacking interactions and H-bond networks [22]. These *s*-triazine polydentate ligands are versatile chelating agents for the synthesis of many metal complexes with interesting molecular and supramolecular structures [23, 24]. Hg(II) and Pb(II) complexes with *bis*(hydrazino)triazine ligands were reported by Ramírez *et al.* [25]. Also, a trigonal bipyramidal mononuclear $[Zn(L')Cl_2]\cdot 2CH_3OH$ complex where **L'** is a hydrazino-*s*-triazine type ligand was synthesized by Yaoting [26]. Eu(III) and Gd(III) complexes of triazine-dihydrazino-tetracetate polydentate ligands were synthesized as powder products by Tei *et al.* [27]. Heptacoordinated Mn(II) complexes of triazines are well known [28] but still not common in literature. Recently, five Mn(II) heptacoordinated complexes with *tris*-pentadentate triazine ligands were presented by Meyer *et al.* [29].

On the other hand, manganese is an essential biometal for many enzymes in biological system [30, 31]. Teslascan (Mangafodipir) was used in medicine for diagnosis as MRI contrast agent while the chemotherapeutic SC-52608 was used as anticancer agent [32]. It is worth to mention that, the overexposure to manganese affect the neurological system leading to a case called manganism [33]. Novel metallodrugs development is a main task in the field of bioinorganic chemistry. In this regard, many Mn-based compounds were found to have interesting in vitro enhanced antimicrobial activity biological activity [34-37]. Also, many Mn-compounds showed promising results as antioxidant [38, 39], anticancer [40-43] and antifungal [44] agents.

Here we reported the synthesis of a new *s*-triazine Schiff base ligand (**L**; **5**; 2-methoxy-4,6-*bis*(2-(pyridin-2-ylmethylene)hydrazinyl)-1,3,5-triazine); (**Scheme 1**) has been introduced. By the reaction of **L** with manganese (II) nitrate tetrahydrate using self-assembly, based on the reaction conditions, two heptacoordinated Mn(II) complexes featuring pentagonal bipyramidal coordination geometry were obtained. The molecular structures of the studied complexes were investigated using single crystal X-ray diffraction combined with density functional theory (DFT) calculations. Also, their antimicrobial activities were presented.

2. Experimental

2.1. Materials

Chemicals were purchased from Sigma-Aldrich Company and were used without further purification.

2.2. Physical measurements

Elemental analyses (CHN) were performed on a Perkin-Elmer 2400 elemental analyzer. FTIR spectra were measured using an Alpha Bruker instrument in KBr pellets (4000-400 cm^{-1}). NMR spectra in DMSO-d_6 were recorded (ppm) on 400 MHz JEOL spectrometer. Thermogravimetric (TGA) measurements were performed on a TGA Q500 instrument under dry nitrogen flow (60 mL min^{-1}). The sample (3–5 mg) is heated (7°C min^{-1}) in an open Al-crucible in the temperature range of 25–800℃.

2.3. Syntheses

The synthetic pathway for the intermediates [13, 45] and the final product (**L; 5)** are shown in **Scheme 1**. *Bis*hydrazino derivative **4** (0.85g, 5mmol) was added portionwise to a hot solution of picolinaldehyde (1.07g, 10 mmol) in 50 mL ethanol in presence of 2-3 drops of acetic acid. The reaction mixture was refluxed for 8hr (the proceeding of the reaction was followed by TLC using MeOH-$CHCl_3$ 9:1). After completion of the reaction, it was left to cool down to room temperature and the precipitated product was collected by filtration, washed with cold ethanol, and dried to obtain the pure product (**L**; **5)** as light yellow powder.

Yield; $C_{16}H_{15}N_9O$ (**L**; **5**) 91%, mp 215-217 ^oC. Anal. Calc. (%): C, 55.01; H, 4.33; N, 36.08. Found: C, 55.02; H, 4.32; N, 36.06. IR (KBr, cm^{-1}): 3424, 3224, 3052, 3011, 2955, 2914, 1625, 1586, 1544 (**Fig. S1**, Supplementary data). ^1H NMR (DMSO-d_6) δ: 3.93 (s, 3H, OCH_3), 7.38 (t, 2H, 2ArH*b*), 7.87-7.92 (m, 4H, 2Ar-$H_{c,d}$), 8.24 (s, 2H, Aldehyde He), 8.58 (d, 2H, 2Ar-H*a*), 11.64 (brs, 2H, 2NH) ppm (**Fig. S2**,

Supplementary data) and ^{13}C NMR (DMSO-d_6) δ: 54.3 OCH_3; 119.7 C4, C4'; 123.9 C2, C2'; 136.9 C3, C3'; 144.5 C6, C6'; 149.2 C1, C1'; 153.3 C5, C5'; 165.7 C8; 171.2 C8, C8' ppm (**Fig. S3**, Supplementary data).

2.3.2. Synthesis of $[MnL(MeOH)NO_3]NO_3$. MeOH; (6)

At room temperature, solid $Mn(NO_3)_2 \cdot 4H_2O$ (~0.251 g, 1 mmol) was added to a solution of **L** (~0.349 g, 1 mmol) in 10 mL methanol. This mixture was left for one day allowed to evaporate slowly at room temperature, the $[MnL(MeOH)NO_3]NO_3$.MeOH; **(6)** complex was formed as yellow crystals.

Yield; $C_{18}H_{23}MnN_{11}O_9$ **(6)** 93%. Anal. Calc. (%): C, 36.50; H, 3.91; N, 26.01. Found: C, 36.49; H, 3.91; N, 26.00. IR (KBr, cm^{-1}): 3428, 3065, 3028, 2947, 2912, 2878, 1644, 1621, 1563, 1543, 1384 (**Fig. S4**, Supplementary data).

2.3.3. Synthesis of $[MnL(H_2O)_2](NO_3)_2$; (7)

10 mL of the ligand (**L**) (~0.349 g, 1 mmol) in methanol and 5mL aqueous $Mn(NO_3)_2 \cdot 4H_2O$ (~0.251 g, 1 mmol) solution were mixed. Complex **7** is formed as pale yellow crystals after two days of slow evaporation.

Yield; $C_{16}H_{19}MnN_{11}O_9$ **(7)** 94%. Anal. Calc. (%): C, 34.05; H, 3.39; N, 27.30. Found: C, 34.09; H, 3.38; N, 27.27. IR (KBr, cm^{-1}): 3427, 3082, 3029, 2916, 2878, 1644, 1621, 1563, 1543, 1384 (**Fig. S5**, Supplementary data).

2.4. Single crystal structure determination

The crystallographic measurements of complexes **6** and **7** were made using a Bruker D8 Quest diffractometer using graphite monochromated Mo-Kα radiation. Absorption corrections were performed by SADABS [46a]. All non-hydrogen atoms were localized on difference Fourier maps and refined in subsequent full-matrix least-squares calculations including anisotropic atomic displacement parameters. All calculations were performed using the Bruker APEX III program system and the SHELXTL program package [46b,c]. The crystallographic data and refinement details are listed in **Table 1**.

2.5. Hirshfeld analysis

Crystal Explorer 17.5 software [47a] is used to perform the Hirshfeld analysis of complexes **6** and **7**. The d_{norm} maps and 2D fingerprint plots were drawn using the same software then utilized to quantify the different intermolecular interactions in the crystal structure of the studied Mn(II) complexes [47b,c].

2.6. Biological studies

2.6.1. Antimicrobial activity

The activity of **L**, complexes **6** and **7** was tested against some different pathogenic microorganisms. *Escherichia coli*, *Staphylococcus aureus*, *Bacillus subtilus*, *Klebsiella pneumoniae*, *Salmonella typhimurium*, and *Pseudomonas aeruginosa* as Gram (-ve bacteria) and *Staphylococcus aureus* as Gram (+ve bacteria) as well as the fungus *Candida albicans* were used for this task. The microorganisms were taken from Bacteriology Lab., Botany Department, Faculty of Science, Tanta University, Egypt. Nutrient agar was prepared for cultivating bacterial cells while, Sabouraud dextrose agar was prepared for *Candida albicans* growing.

The tested compounds were checked for their activity by cut plug method [48] against different microbes. The amounts of 0.5 mL (about10^5 cells/mL) were speared over plate of corresponding sterilized media. In the seeded agar plate, wells were made by a 6 mm cork-borer and filled with 200µL of the tested compound (15 mmol/L), then were incubated at 37° C for 3 days. The obtained results (inhibition zone) were measured and compared with fluconazole and gentamicin (15mmol/L) as standard antifungal and antibacterial agents, respectively [48]. Moreover, different dilutions from each compound was prepared in one mL of sterile nutrient broth which were used to determine the minimal inhibition concentrations (MICs) against different microbes as described by Ter-Laak *et al*. [49].

2.6.2. Surviving ratio of tested microorganisms

0.5 mL of suspended microorganisms and 9.5 mL nutrient broth includes the examined compounds (5, 10 and 15 mmol/L) were mixed in a sterile tube. The inoculated slants were incubated overnight at 37° C with shaking at 250 rpm. 0.1 mL from the resulting mixture is diluted by a two-fold factor, spread over the agar plate, and then incubated for one day at the same temperature. On other hand, control was done using the same procedure but without the examined compounds. The number of colony forming units (CFU) was counted then the surviving ratios (M/C) were determined at each concentration and for every microbe. The C and M are the number of organisms in absence and presence of the examined compounds, respectively.

2.6.3. Effect on cell permeability "leakage of potassium"

Cells of *Escherichia coli*, *Candida albicans* and *Staphylococcus aureus* were separated by centrifugation after growing for 2 days, and washed with sterile water. Then, cells were distributed in sterile water followed by 30 minutes shaking. The cells

are separated and mixed with 10 mL of the examined compounds (5, 10 and 15 mmol/L). After incubation for 1 day, cells were separated and K^+ in solution was measured using Flame photometer Model CoRNing M 410-Sherwood Scientific Ltd.

3. Computational details

All calculations were carried out using Gaussian 09 software package [50]. At the X-ray structure coordinates of complexes **6** and **7**, single point calculations using WB97XD and MPW1PW91 methods [51] combined with TZVP basis sets [52] were performed at the unrestricted level with multiplicity of 6. Atoms in molecules (AIM) [53] and natural bond orbital (NBO) calculations were performed using Multiwfn [54a] and NBO 3.1 [54b] programs, respectively.

4. Results and discussion

4.1. X-ray structure description

The $[MnL(MeOH)NO_3]NO_3$.MeOH complex (**6**) crystallized in the centrosymmetric triclinic space group P-1 with one formula unit per asymmetric unit and Z = 2. The structure of complex **6** is shown in **Fig. 1** while list of bond lengths (Å) and angles (°) are given in **Table 2**. The asymmetric unit consists of one complex $[MnL(MeOH)NO_3]^+$ cation, one nitrate counter anion and one crystallized methanol molecule. The Mn(II) is coordinated with one *s*-triazine ligand (**L**), one monodentate nitrate *via* one of its O-atoms and one methanol molecule. The molecular structure of complex **6** has a single heptacoordinated Mn(II) ion with a distorted pentagonal bipyramidal environment. The ligand **L** acts as a pentadentate chelator *via* five N-atoms in the basal plane: four short Mn-N interactions (Mn1-N1 (2.294(2) Å), Mn1-N5 (2.366(2) Å), Mn1-N8 (2.385(2) Å), Mn1-N6 (2.398(2) Å)) and one significantly longer Mn1-N7 (2.544(2) Å) bond. The Mn-N distances increase in the sequence: Mn-N(triazine)<Mn-N(hydrazone)< Mn-N(pyridine) ongoing to the outside along the chelate arms. Also, the two Mn-N(pyridine) distances are different (0.145 Å) and the structure seems to be twisted at the end of the pincer array. The reason could be simply explained due to the steric repulsion between the two H-atoms (2.122 Å) at the pyridyl-6 positions. As a result, the angle between the N1–N5–N6–Mn1 and N1–N8–N7–Mn1 planes is 10.78°. This twist at the end of the ligand arms lead to longer Mn1-N7 bond compared to Mn1-N6 one. The coordinated nitrate ion and methanol molecules forming the two axial Mn-O1 (2.187(2)) and Mn-O3 (2.1741(19)) bonds which showed strong deviation from linearity with O1-Mn1-O3 angle of 154.48(7)º.

The complex units are packed in the crystal structure *via* set of strong N-H…O and O-H…O hydrogen bonds combined with weak C-H…O interactions. These interactions are given in **Table 3** while **Fig. S6** (Supplementary data) showed only the most important hydrogen bond contacts. **Fig. 2A** showed the wavy-like hydrogen bond chain in which the complex cations, crystallized methanol molecules and nitrate anions are connected alternatively by the N-H…O and O-H…O hydrogen bonds. The coordinated methanol molecule connects two of this chain *via* the O1-H1…O6 hydrogen bonds (2.718(3) Å) leading to the formation of the two dimensional hydrogen bond network shown in **Fig. 2B**.

Interestingly, the nitrate counter anion makes some interactions with one carbon from the adjacent pyridyl group with C10…N11 and C10…O6 distances of 3.100 Å and 3.164 Å, respectively, which further support the twist of the pyridine moieties from one another at the end of the pincer array. On the other hand, the coordinated nitrate anion forms one short C15...O4 (2.974 Å) contact with the Schiff base moiety (**Fig. 3**).

The $[MnL(H_2O)_2](NO_3)_2$; (**7**) complex crystallized in the centrosymmetric monoclinic space group P121/n1 with two formula units per asymmetric unit. The structure of complex **7** is shown in **Fig. 4** and list of bond lengths (Å) and angles (°) for this complex are given in **Table 4**. The coordination sphere of both units built from one pentadentate *N*-chelate (**L**) and two axial Mn-O bonds. In this case the two axial Mn-O bonds are from two coordinated water molecules while the two nitrate counter anions are freely uncoordinated. Similar to complex **6**, the heptacoordinated Mn(II) in **7** has a distorted pentagonal bipyramidal configuration. In addition, the Mn-N distances increases ongoing from the triazine moiety through the two arms of the pincer ligand. In unit **1** of this complex, the two Mn-N(pyridine) bond distances are 2.409(3) and 2.415(4) for Mn1-N6 and Mn1-N7, respectively, and the H-atoms at the pyridyl-6 positions make a distance of 2.201 Å while the torsion angle between the two N1-N5-N6-Mn1 and N1-N8-N7-Mn1 planes is 9.13º. In the second formula unit, the two Mn-N(pyridine) bonds are longer (Mn2-N15: 2.436(3) and Mn2-N16: 2.516(4)) and the H...H contact distance is shorter (2.133 Å) while smaller dihedral angle between the two N10-N14-N15-Mn2 and N10-N17-N16-Mn2 planes is observed (6.84º), compared to the first unit. One could conclude from these results that, the two strong Mn-N(pyridine) bonds (as in unit 1) assisted the higher twist of the two pyridyl ends from one another which increase the H...H contact distance.

In the solid state structure of **7**, the $[MnL(H_2O)_2]^{2+}$ cationic parts of the complex and the anionic nitrate groups are connected by the hydrogen bonds shown in **Fig. 5A**. List of the most important H-bonds in **7** are given in **Table 5**. It can be seen from this figure that the coordinated water, hydrazone NH groups of the ligand molecules and the nitrate counter anions are involved in the hydrogen bonding interactions forming the three dimensional hydrogen bond network shown in **Fig. 5B**. The N-H…N hydrogen bonds connect the organic ligands in two neighboring complex units which occurred between the hydrazone moiety as proton donor (NH) from one ligand unit and one of the free nitrogen atoms in the triazine ring from the neighboring complex unit. For more clarity, those are labeled V (2.960(4) Å) and VI (2.976(4) Å) in **Fig. 5A** and **Table 5**. Moreover, the N-H…O hydrogen bonds occurs between the other two NH groups from the hydrazone moieties and the O-atoms from the free nitrate anions (I and X). The rest of H-bonds occurred between the coordinated water molecules and the nitrate anions. The O-H…O hydrogen bonds are responsible for connecting the complex units along the crystallographic *b*-direction and shared together with the N-H…N hydrogen bonds to connect the molecules along the *c*-direction leading to the two dimensional layers formed along the *bc*-plane which are further connected via alternative N-H…O and O-H…O hydrogen bonds along the *a*-direction forming the 3D hydrogen bond network shown in **Fig. 5B**.

Similar to **6**, this complex showed some anion-π stacking interactions occurred between the oxygen atoms from the nitrate counter anions and the carbon atoms either from the *s*-triazine or the pyridine moieties. The shortest C...O contacts in the crystal structure of **7** are C21...O12 (3.096 Å), C17...O15 (3.121 Å) and C19...O14 (3.102 Å).

4.2. Hirshfeld analysis

The Hirshfeld analyses shed the light on the frequency and strength of all interactions in the crystal structure of complexes **6** and **7** [55] (**Figs. S7-S9**; Supplementary data). The percentages of all possible interactions are summarized graphically in **Fig. 6**. It is clear from the presented data that, the O…H hydrogen bonding interactions have the highest contribution among the intermolecular contacts. The O…H interactions significantly contributed by 41.7% of the whole fingerprint (FP) plot in complex **6** while 40.7 and 41.8% in case of units **1** and **2** of complex **7**, respectively. The results are quite comparable in both complexes. These interactions appeared as intense red spots and sharp spikes in d_{norm} maps and FP plots, respectively (**Fig. S8**, Supplementary data). Although both complexes showed comparable amount of N...H

hydrogen bonding interactions but the decomposed FP plot and d_{norm} maps (**Fig. S9**, Supplementary data) revealed that these interactions are significantly stronger in complex **7** than **6**. While the N...H interactions appeared as broad spikes in the FP plot and blue regions in the d_{norm} map of complex **6**, these interactions showed sharp spikes and intense red spots in the FP plot and d_{norm} map, respectively, in **7** indicating that these interactions have short contact distances and are considered strong. Moreover, the percentages of the C...O contacts are 1.7 and ~4.3% in complexes **6** and **7**, respectively. Those appeared as very fad red spots indicating that these interactions are considerably weak. Moreover, negligible C…C contacts, absence of complementary red and blue triangles in the shape index plots and absence of green flat areas in the curvedness plot gave strong indications on the absence of any significant π-π stacking interactions.

4.3. AIM and NBO Analyses

The AIM [53] results have been utilized for complexes **6** and **7** to explore the nature and strength of the various metal-ligands interactions in terms of the topological parameters at the corresponding (3, -1) bond critical points [56-59]. The results of the AIM analysis, of the coordination bonded interactions between Mn(II) and donor atoms for the studied complexes are presented in **Table S1** (Supplementary data). Closed-shell interactions are characterized by low electron density (ρ(r)) values [60] and small positive value of laplacian of electron density ($\nabla^2\rho(r)$) [61]. The opposite is almost true for the shared interactions [60, 62]. All Mn-N and Mn-O interactions showed (3, -1) bond critical point at the corresponding bond paths and the values of the topological parameters ρ(r) and $\nabla^2\rho(r)$ are consistent with the closed-shell character of these bonds (**Table S1**; Supplementary data). Generally, larger ρ(r) and $\nabla^2\rho(r)$ values result in stabilization of the structure [63]. **Fig. 7** showed a nice inverse linear relationship between Mn-N/Mn-O distances with these topological parameters (ρ(r) and $\nabla^2\rho(r)$) as well as the interaction energies calculated using the Espinosa relation [64, 65]. On other hand, the positive H(r) and potential to kinetic energy density (|V(r)|/G(r)) very close to 1 confirm the low covalent characters of these interactions and they are mainly have the characteristics of closed shell interactions [66].

The net charges at Mn, nitrate anion, methanol and the ligand **L** were calculated with the aid of NBO method (**Table 6**). The charges at the manganese central atom are less

than +2 as a result of the negative charge density transferred from the coordinated ligands to Mn(II). The net electron density transferred to the central metal atom are 0.846 e for complex **6** and 0.897 e and 0.880 e for units **1** and **2** of complex **7**, respectively. Here we taken the average values of the natural charges calculated using both methods as the results are very comparable. While the ionic nitrate groups have natural charges very close to -1, the coordinated nitrate has natural charge of -0.785e (average value). Hence, the latter loses ~0.215 e to the Mn(II) ion in complex **6**, the corresponding values in case of complex **7** are almost zero. In complex **7**, higher amount of electron density transferred from the ligand (**L**) to Mn(II) compared to **6**. In the latter, there is one anionic ligand (nitrate) coordinated to Mn(II) which significantly deplete its positive charge. As a result, smaller amount of electron density transferred from the ligand (**L**) to Mn(II) compared to **7**. Also, the strongly coordinated water molecules- those having shorter Mn-O distances- transferred higher amount of electron density (0.1639-0.1655 e) to the Mn(II) compared to the weakly coordinated ones (0.1249-0.1330e). The coordinated methanol transferred the least amount of electrons to the metal ion compared to the rest of the O-donor ligands (NO_3^- and H_2O).

The interaction energies ($E^{(2)}$) due to the intramolecular charge transference occur between the ligands donor atoms and Mn(II) are given in **Tables S2-S3** (Supplementary data) and summary of these results are given in **Table 7**. Since we deal with the studied systems, based on the energy analyses (**Table S4**, Supplementary data), as high spin complexes which is also supported by literature for similar Mn(II) complexes [29] with the electron-deficient *s*-triazine ring which has weak ligand field strength [67]. So; calculations are based on the high spin state with five unpaired electrons and multiplicity of 6 and the intramolecular charge transfer interactions will be described in terms of the alpha and beta orbitals of the studied systems. The presented results agree well with the X-ray structure analysis where the Mn-N interactions becomes more weak ongoing from the triazine moiety to outside the two ligand arms (**Table 7**).

Presentations of the most important interactions between the occupied ligand donor atoms NBOs as electron donor and the acceptor anti-bonding Mn(II) natural bond orbitals are shown in **Fig. 8**. The first important information that could be deduced from this figure is that, the LP(1)O are almost parallel to the plane containing Mn-atom and hence weakly interacting with the Mn-antibonding orbitals. In contrast, the

second lone pairs of O-atoms (LP(2)O) are nearly perpendicular to the plane containing the Mn-atom, hence are strongly interacting with its orbitals. This in line with the significantly higher interaction energies of the LP(2)O→LP*Mn compared to LP(1)O→LP*Mn ones (**Tables S2-S3**, Supplementary data). All the ligand (**L**) NBOs are clearly oriented towards the central metal atom, hence are strongly interacted with the metal anti-bonding orbitals, which stabilize the chelate structure of the complex. Analysis of the Mn-antibonding natural orbitals indicated that the alpha LP*(6)Mn and beta LP*(1)Mn NBOs have mainly s-orbital characters as indicated from the almost spherical shape of electron density. The rest of the alpha and beta NBOs have mixed p- and d-orbital characters.

4.4. Vibrational Spectra and TGA Analysis

The FTIR spectra of the free ligand (**L**) and its Mn(II) complexes are shown in (**Figs. S1, S4 and S5**; Supplementary data). The vibrational bands at 3424 cm^{-1} and 3224 cm^{-1} in the IR spectrum of the free ligand are assigned to the $\nu_{(N-H)}$ modes of the hydrazone NH groups. In case of the Mn(II) complexes, the broad band appeared at ~3427 cm^{-1} which masked the $\nu_{(N-H)}$ modes is considered as a combination of the $\nu_{(O-H)}$ modes of coordinated and crystallized water/methanol molecules. The IR spectra of the ligand reveal absorption bands characteristic for $\nu_{(C=N)}$ and $\nu_{(C=C)}$ stretching modes at 1625 cm^{-1} and 1586-1544 cm^{-1}, respectively. Both vibrational modes are shifted to higher wavenumbers in case of the studied complexes. The $\nu_{(C=N)}$ appeared as splitted band in the wavenumber region of 1621-1644 cm^{-1} while the $\nu_{(C=C)}$ vibrations are shifted to 1543-1563 cm^{-1}. The free ligand showed the aromatic and aliphatic C-H vibrations in the range 3052-3011 and 2955-2914 cm^{-1}, respectively. These modes appeared at 3082-3028 and 2947-2878 cm^{-1}, respectively, in case of the Mn(II) complexes. The appearance of a new strong sharp band at 1384 cm^{-1}, is characteristic for the presence of the nitrate ion. The rest of the nitrate vibrations could not be well distinguished as they found overlapped with the ligand vibrations.

Thermogravimetric analysis of the ligand and its two Mn(II) complexes are shown in **Fig. S10** (Supplementary data). The ligand showed low thermal stability and starts to decompose gradually at ~60 ºC in several successive steps. The complexation between Mn(II) and **L** increases the thermal stability where complexes **6** and **7** started to decompose at higher temperature. Complex **6** starts to lose the crystal solvent first at about 80°C followed by small step, probably corresponding to the loss of the coordinated methanol while complex **7** showed clear step at about 130 °C

corresponding to the loss of the coordinated water molecules followed by the ligand decomposition in both complexes at about 201-209 °C in a very similar fashion to the decomposition of the free ligand itself but at higher temperature.

4.5. Antimicrobial activity of L, 6 and 7

Initial assessment of the antimicrobial activity of **L** and its Mn(II) complexes on the studied microorganisms is determined. The diameters of the resulting inhibition zones are given in **Table 8** and representative example for the biological experiments is shown in **Fig. S11** (Supplementary data).

The studied compounds showed inhibition zones with different sizes indicating their good antibacterial and antifungal activities against the tested microorganisms compared to the well-known antibacterial gentamycin and the antifungal fluconazole, respectively. This obvious effect could be attributed to the presence of different side chains such as methoxy group (OCH_3), pyridine rings and hydrazone groups attached to the triazine moiety as well as the presence of transition metal ion (Mn(II)); all have direct effects on the biological activity. For the studied microorganisms, the free ligand (**L**) showed inhibition zones with smaller sizes than the corresponding Mn(II) complexes. This dissimilarity might be due to the extent of interactions between the examined compounds and the tested organisms [68]. The presence of Mn(II) in the structure clearly modulate the biological activity of the ligand. Mn(II) plays an important role in the redox reactions occurred the biological systems of microorganisms [69, 70]. Also, it acts as a chemical oxidant and microbial inhibitor [71].

Further biological test which confirmed the antimicrobial action of the studied compounds, is the surviving ratio experiment. It showed the effect of compound concentration on the surviving ratio. The results of the surviving ratio experiments are presented graphically in **Fig. 9**. It is clear that as the concentration of the synthesized chemical compounds increased, the inhibitory effect increased. The studied compounds killed about 80–95% of the tested microorganisms at a concentration of 15 mmol/L. In case of the lowest concentration (5 mmol/L), the compound inhibition potency was in the range of 30-50% (**Fig. 9**).

Moreover, the MICs of the examined compounds (**L**, **6** and **7**) against selected microbes were determined and the results are collected in **Table 9**. Based on these result, complex **7** could be the best candidate as antifungal against *C. albicans* while the ligand (**L**) is the best as antibacterial agent compared to the others.

This reactivity of microorganism's growth inhibition may be due to its interaction with the compound side chains which affect the impermeability of the cell wall [72-74]. As a result, cell wall disruption occurs and the ability of the microorganism's cell wall to control K^+ ion becomes less. Here we tested the effect of the complex **6** concentration on the potassium ion flow (**Fig. 10**). The results revealed the presence of clear changes in the K^+ flow with the concentration of **6**. The flow of K^+ is higher by 0.27-0.39 ppm for the treated cells compared to control which revealed that **6** lead to increase the K^+ leakage from different cells. The increases in the compound concentration increased the K^+ leakage up to 0.45 ppm. These results gave a good indication on the effect of the studied compounds on the impermeability of the cell wall [75, 76].

5. Conclusion

Depending on medium, the two heptacoordinated manganese(II) complexes $[MnL(MeOH)NO_3]NO_3$. MeOH; (**6**) and $[MnL(H_2O)_2](NO_3)_2$; **7** with *s*-triazine *bis*-Schiff base chelating ligand (**L**) were synthesized and their molecular structure aspects were analyzed using FTIR spectra, X-ray diffraction combined with DFT calculations. Complex **6** is formed when solid Mn(II)-nitrate is added to the ligand solution (**L**) in methanol, while **7** is formed from the mixed aqueous/methanolic solution. Both complexes showed distorted pentagonal bipyramidal configuration around the Mn(II) ion. The two ligand (**L**) arms become twisted at their ends (pyridine moiety) due to the short H...H distances at the pyridyl 6-position. It is found that, the Mn-N(triazine)>Mn-N(hydrazone)>Mn-pyridine according to the strength of interaction. The nature of the Mn-N and Mn-O bonds is analyzed using AIM and NBO methods. The presence of the strong and sharp band at 1384 cm^{-1} confirms the presence of nitrate group in both complexes. Both complexes thermally decomposed at higher temperature compared to the ligand. The ligand (**L**), complexes **6** and **7** showed good antibacterial and antifungal activities. Complex **7** is recommended to use as antifungal agents against the fungus *C. Albicans*.

CONFLICTS OF INTEREST

The authors declare that they have no conflict of interest.

ACKNOWLEDGMENTS

The authors extend their appreciation to the Deanship of Scientific Research at King Saud University for funding this work through Research Group no. RGP-234, Saudi Arabia.

References

[1] a) M. Albrecht, Angew. Chem. Int. Ed., 38 (1999) 3463; b) F.A. Cotton, C. Lin, C.A. Murillo, Acc. Chem. Res., 35 (2002) 565.

[2] F. Hof, S.L. Craig, C. Nuckolls, J. Rebek, Angew. Chem. Int. Ed., 41(2002) 1488.

[3] N.C. Desai, A.H. Makwana, R.D. Senta, J. Saudi Chem. Soc., 20 (2016) 686.

[4] T. Vilaivan, N. Saesaengseerung, D. Jarprung, S. Kamchonwongpaisan, W. Sirawaraporn, Y. Yuthavong, Bioorg. Med. Chem., 11 (2003) 217.

[5] T. Lübbers, P. Angehrn, H. Gmünder, S. Herzig, J. Kulhanek, Bioorg. Med. Chem. Lett., 10 (2000) 821.

[6] J. N. Sangshetti, D.B. Shinde, Bioorg. Med. Chem. Lett., 20 (2010) 742.

[7] W. Lv, B. Banerjee, K.L. Molland, M.N. Seleem, A. Ghafoor, M.I. Hamed, B. Wan, S.G. Franzblau, A.D. Mesecar, M. Cushman, Bioorg. Med. Chem., 22 (2014) 406.

[8] K.K. Bansal, D. Kakde, U. Gupta, N.K. Jain, J. Nanosci, Nanotechnol., 10 (2010) 8395.

[9] R. Shanmugakala, P. Tharmaraj, C.D. Sheela, C. Anitha, Int. J. Inorg. Chem., 2012 (2012) 1.

[10] N.S. Mewada, D.R. Shah, H.P. Lakum, K.H. Chikhalia, J. Assoc. Arab Univ. Basic Appl. Sci., 20 (2016) 8.

[11] M. Easson, B. Condon, M. Yoshioka-Tarver, S. Childress, R. Slopek, J. Bland, T.M. Nguyen, S.C. Chang, E. Graves, AATCC Rev., 11 (2011) 60.

[12] V.V. Nedel'ko, A.V. Shastin, B.L. Korsunskii, N.V. Chukanov, T.S. Larikova, A.I. Kazakov, Russ. Chem. Bull. 54 (2005) 1710.

[13] A. El-Faham, Kh. A. Dahlous, Z. A. AL Othman, H. A. Al-Lohedan, G. A. El-Mahdy, Molecules, 21 (2016) 436.

[14] G. Blotny, Tetrahedron, 62 (2006) 9507.

[15] M. Arshad, T.A. Khan, M.A. Khan, ChemInform., 46 (2015) 110.

[16] C.A.M. Afonso, N.M.T. Lourenco, A.d.A. Rosatella, Molecules, 11 (2006) 81.

[17] L. Pavelek, V. Ladányi, M. Nečas , S. Vallová, K. Wichterle, Polyhedron, 107 (2016) 89.

[18] Z.J. Kaminski, Biopolymers, 55 (2000) 140.

[19] J.T. Thurston, J.R. Dudley, D.W. Kaiser, I. Hechenbleikner, F.C. Schaefer, D. Holm-Hansen, J. Am. Chem. Soc., 73 (1951) 2981.

[20] Q. Zhang, C. He, P. Yin, J.M. Shreeve, Chem. Asian J., 9 (2014) 212.

[21] P. Gamez, J. Reedijk, Eur. J. Inorg. Chem., 2006 (2006) 29.

[22] a) S. Demeshko, S. Dechert, F. Meyer, J. Am. Chem. Soc., 126 (2004) 4508; b) J.A. Zerkowski, C.T. Seto, G.M. Whitesides, J. Am. Chem. Soc., 114 (1992) 5473.

[23] J.R. Galan-Mascaros, J.M. Clemente-Juan, K.R. Dunbar. J. Chem. Soc., Dalton Trans., (2002) 2710.

[24] R. Wietzke, M. Mazzanti, J.M. Latour, J. Percaut. Inorg. Chem., 38 (1999) 3581.

[25] J. Ramírez, A.-M. Stadler, L. Brelot, J.-M. Lehn, Tetrahedron, 64 (2008) 8402.

[26] F. Yaoting, L. Gang, L. Zifeng, H. Hongwei, M. Hairong, J. Mol. Struct., 693 (2004) 217.

[27] L. Tei, M. Benzi, F. Kielar, M. Botta, C. Cavallotti, G.B. Giovenzana, S. Aime, Helv. Chim. Acta, 92 (2009) 2414.

[28] a) G.-Y. Hsu, P. Misra, S.-C. Cheng, H.-H. Wei, S. Mohanta, Polyhedron, 25 (2006) 3393; b) M. Zhang, R. Fang, Q. Zhao, J. Chem. Crystallogr., 38 (2008) 601 and c) P. Tyagi, U. P. Singh, J. Coord. Chem., 62 (2009) 1613.

[29] A. Das, S. Demeshko, S. Dechert, F. Meyer, Eur. J. Inorg. Chem., 2011 (2011) 1240.

[30] E. J. Larson, V. L. Pecoraro, in: V.L. Pecoraro (Ed.), Manganese Enzymes, VCH Publishers Inc, New York, 1992, 1–28.

[31] C. S. Mullins, V. L. Pecoraro, Coord. Chem. Rev., 252 (2008) 416.

[32] Z. Guo, P. J. Sadler, Angew. Chem. Int. Ed., 38 (1999) 1512.

[33] D. S. Avila, R. L. Puntel, M. Aschner, Met. Ions Life Sci., 13 (2013) 199.

[34] P. Dorkov, I. Pantcheva, W. Sheldrick, H. Figge, R. Petrova, M. Mitewa, J. Inorg. Biochem., 102 (2008) 26.

[35] S. Mandal, A. Rout, A. Ghosh, G. Pilet, D. Bandyopadhyay, Polyhedron, 28 (2009) 3858.

[36] M. Zampakou, M. Akrivou, E.G. Andreadou, C.P. Raptopoulou, V. Psycharis, A. A. Pantazaki, G. Psomas, J. Inorg. Biochem., 121 (2013) 88.

[37] M. Zampakou, S. Balala, F. Perdih, S. Kalogiannis, I. Turel, G. Psomas, RSC Adv., 5 (2015) 11861–11872.

[38] M. Zampakou, A.G. Hatzidimitriou, A.N. Papadopoulos, G. Psomas, J. Coord. Chem., 68 (2015) 4355.

[39] M. Zampakou, N. Rizeq, V. Tangoulis, A.N. Papadopoulos, F. Perdih, I. Turel, G. Psomas, Inorg. Chem., 53 (2014) 2040.

[40] D. Zhou, Q. Chen, Y. Qi, H. Fu, Z. Li, K. Zhao, J. Gao, Inorg. Chem., 50 (2011) 6929.

[41] Y. Li, J. Zhao, C. He, L. Zhang, S. Sun, G. Xu, J. Inorg. Biochem., 150 (2015) 28.

[42] D. A. Megger, K. Rosowski, C. Radunsky, J. Kösters, B. Sitek, J. Müller, Dalton Trans., 46 (2017) 4759.

[43] Q. Qin, T. Meng, Z. Wei, C. Zhang, Y. Liu, H. Liang, Z. Chen, Eur. J. Inorg. Chem., (2017) 1824.

[44] D. P. Singh, K. Kumar, C. Sharma, Eur. J. Med. Chem., 45 (2010) 1230.

[45] a) H. Tanaka, A. Wada, M. Shiro, K. Hioki, D. Morisaki, M. Kunishima, Heterocycles, 79 (2009) 609 and b) L. Pavelek , V. Ladányi, M. Nečas , Z. Moravec, K. Wichterle, Polyhedron, 119 (2016) 134.

[46] a) G. M. Sheldrick, SADABS. Program for empirical absorption correction of area detector data, University of Göttingen, Germany, 1996; b) G. M. Sheldrick, Acta Cryst., A71 (2015) 3 and c) A. L. Spek, Acta Cryst., D65 (2009) 148.

[47] a) M. J. Turner, J. J. McKinnon, S. K. Wolff, D. J. Grimwood, P. R. Spackman, D. Jayatilaka, M. A. Spackman, Crystal Explorer17 (2017) University of Western Australia. http://hirshfeldsurface.net; b) M. A. Spackman, J. J. McKinnon, Cryst. Eng. Comm., 4 (2002) 378; c) J. J. McKinnon, D. Jayatilaka, M. A. Spackman, Chem. Commun., (2007) 3814.

[48] T. G. Pridham, L. A. L. Felser, O. L. Shorweel, F. Stodola, Bendict, R. G. C. Foley, P. W. Jacks, W. J. Zaumeyer, W. H. Perston, J. W. Mitchell, Phytopathol, 46 (1956) 568.

[49] E.A.Ter-Laak, A. Pijpers, J.H. Noordergraaf, E.C. Schoevers, J.H. Verheijden, Antimicrob. Agents Chemother., 35 (1991) 228.

[50] M.J. Frisch, G.W. Trucks, H.B. Schlegel, G.E. Scuseria, M.A. Robb, J.R. Cheeseman, G.Scalmani, V.Barone, B.Mennucci, G.A. Petersson, H.Nakatsuji, M. Caricato, X. Li, H.P. Hratchian, A.F. Izmaylov, J.Bloino, G.Zheng, J.L. Sonnenberg, M. Hada, M. Ehara, K. Toyota, R. Fukuda, J. Hasegawa, M. Ishida, T. Nakajima, Y. Honda, O. Kitao, H. Nakai, T. Vreven, J.A. Montgomery, Jr., J.E. Peralta, F. Ogliaro, M. Bearpark, J.J. Heyd, E. Brothers, K.N. Kudin, V.N. Staroverov, R. Kobayashi, J. Normand, K. Raghavachari, A. Rendell, J.C. Burant, S.S. Iyengar, J. Tomasi, M. Cossi, N. Rega, J.M. Millam, M. Klene, J.E. Knox, J.B. Cross, V. Bakken, C. Adamo, J. Jaramillo, R. Gomperts, R.E. Stratmann, O. Yazyev, A.J. Austin, R. Cammi, C.

Pomelli, J.W. Ochterski, R.L. Martin, K. Morokuma, V.G. Zakrzewski, G.A. Voth, P. Salvador, J.J. Dannenberg, S. Dapprich, A.D. Daniels, O. Farkas, J.B. Foresman, J.V. Ortiz, J. Cioslowski, D.J. Fox, Gaussian, Inc., Wallingford CT, 2009.

[51] a) J. D. Chai, M. Head-Gordon, Phys. Chem. Chem. Phys., 10 (2008) 6615 and b) C. Adamo, V. Barone, J. Chem. Phys., 108 (1998) 664.

[52] a) A. Schaefer, H. Horn, R. Ahlrichs, J. Chem. Phys., 97 (1992) 2571 and b) A. Schaefer, C. Huber, R. Ahlrichs, J. Chem. Phys., 100 (1994) 5829.

[53] R. F. W. Bader, Atoms in Molecules: A Quantum Theory, Oxford University Press, Oxford, U.K., 1990.

[54] a) T. Lu, F. Chen, J. Comp. Chem., 33 (2012) 580; b) E.D. Glendening, A.E. Reed, J.E. Carpenter, F. Weinhold, NBO Version 3.1, CI, University of Wisconsin, Madison, 1998.

[55] a) M. A. Spackman, D. Jayatilaka, Cryst. Eng. Comm., 11 (2009) 19; b) F. L. Hirshfeld, Theor. Chim. Acta, 44 (1977) 129.

[56] C. F. Matta, J. Hernandez-Trujillo, T.-H. Tang, R. F. W. Bader, Chem. Eur. J., 9 (2003) 1940.

[57] S. J.Grabowski, A. Pfitzner, M. Zabel, A. T. Dubis, M. Palusiak, J. Phys. Chem. B, 108 (2004) 1831.

[58] C. F. Matta, N. Castillo, R. J. Boyd, J. Phys. Chem., A 109 (2005) 3681.

[59] A. M. Pendás, E. Francisco, M. A. Blanco, C. Gatti, Chem. Eur. J., 13 (2007) 9362.

[60] R. F. W. Bader, H. Essén, J. Chem. Phys., 80 (1984) 1943.

[61] R. G. A. Bone, R. F. W. Bader, J. Phys. Chem., 100 (1996) 10892.

[62] M. F. Bobrov, G. V. Popova, V. G. Tsirelson, Russ. J. Phys. Chem., 80 (2006) 584.

[63] a) C. Gatti, Z. Kristallogr., 220 (2005) 399; b) G. V. Gibbs, R. T. Downs, D. F. Cox, N. L. Ross, M. B. Boisen, K. M. Rosso, J. Phys. Chem. A, 112 (2008) 3693.

[64] E. Espinosa, E. Molins, C. Lecomte, Chem. Phys. Lett., 285 (1998) 170.

[65] I. Love, J. Phys. Chem. A, 113 (2009) 2640.

[66] D. Cremer, E. Kraka, Angew. Chem. Int. Ed., 23 (1984) 627.

[67] E.A. Medlycott, K.A. Udachin, G.S. Hanan, Dalton Trans., (2007) 430.

[68] I. Tuney, B.H. Cadiric, D. Unal, A. Sukatar, Fres. Environ. Bullt., 16 (2007) 428.

[69] R. Wetzel, Limnology: Lake and River Ecosystems. Academic Press, San Diego, CA, 2001.

[70] C. A. Nealson, K. H. Saffarini, Ann. Rev. Microbiol., 48 (1994) 311.

[71] C. G. Gabelich, W. Fredrick, W. R. Knocke, C. L. Connie, American Water Works Association, 98 (2006) 116.

[72] Y. S. Kim, H. W. Kim, S. H. Lee, K. S. Shin, Int. J. Biol. Macromol., 41 (2007) 36.

[73] S.Venkataraman, Y. Zhang, L. Liu, Y.Y. Yang, Biomaterials, 31 (2010) 1751.

[74] G. Lu, D. Wu, R. Fu, React. Funct. Polym., 67 (2007) 355.

[75] N. Kawabata, M. Nishiguchi, Appl. Environ. Microb., 54 (1988) 2532.

[76] A. Popa, C. M. Davidescu, R.Trif, G. H. Ilia, S. Iliescu, G. H. Dehelean, React. Funct. Polym., 55 (2003) 151.

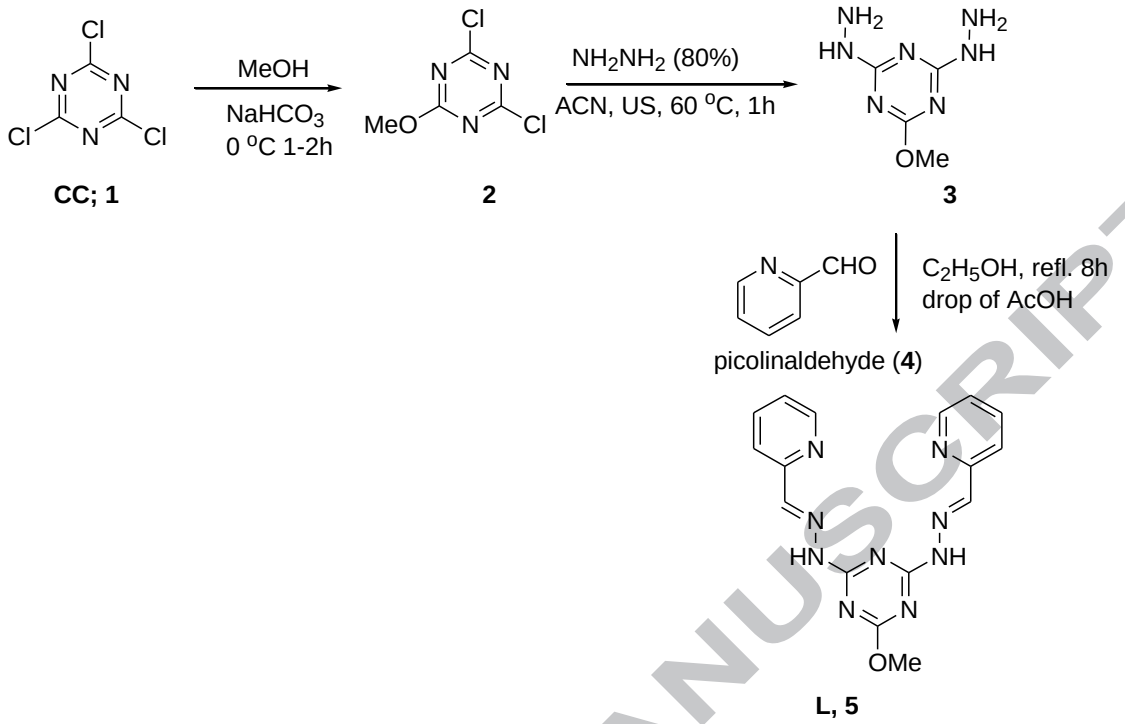

Scheme 1 Synthesis of the 1,3,5-triazine-based chelating ligand (**L**; **5**).

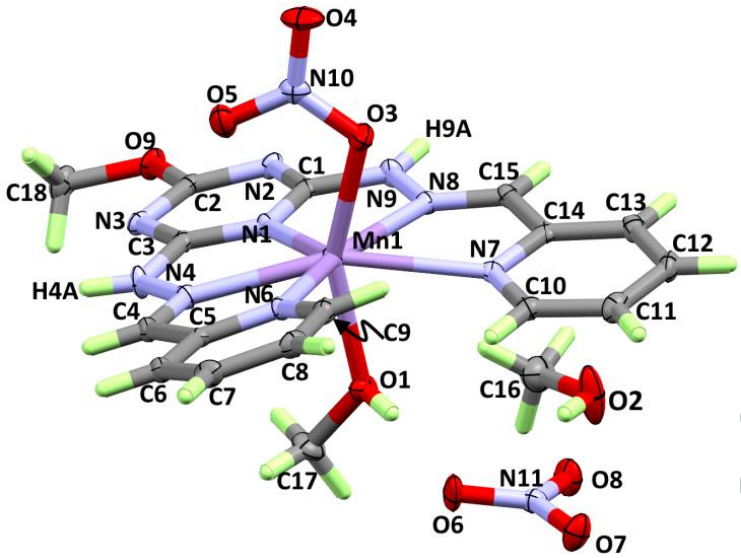

Fig. 1 Thermal ellipsoids at 50% probability of the asymmetric unit and atom numbering scheme of [MnL(MeOH)NO_3]NO_3.MeOH; **6**.

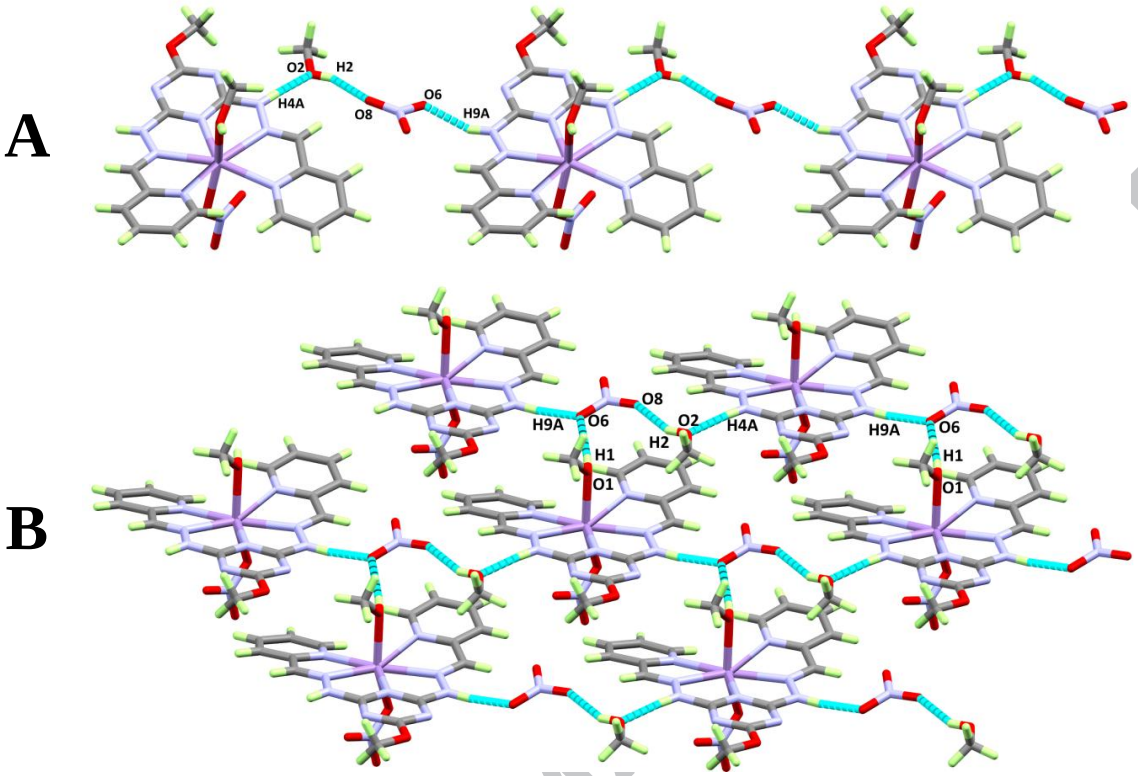

Fig. 2 The wavy-like hydrogen bond chain (**A**) are connected *via* O1-H1…O6 hydrogen bonds leading to the two dimensional hydrogen bond network (**B**).

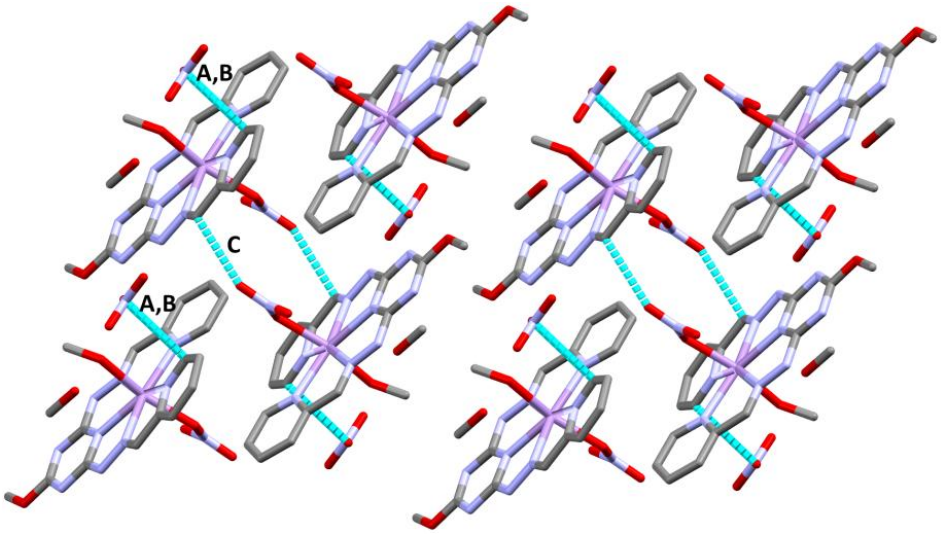

Fig. 3 View along the crystallographic *c*-direction showing the anion-aromatic stacking interactions *via* C…N and C…O contacts. All hydrogen atoms are omitted for more clarity. A) C10…N11 (3.100(3) Å); B) C10…O6 (3.164(3) Å), and C) C15...O4 (2.974(3) Å).

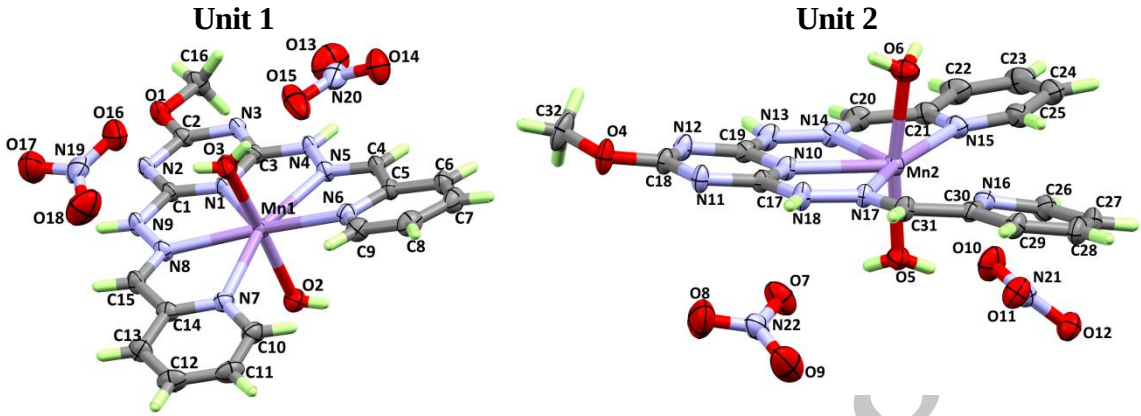

Fig. 4 Thermal ellipsoids at 30% probability of the asymmetric unit and atom numbering scheme of $[MnL(H_2O)_2](NO_3)_2$; **7**.

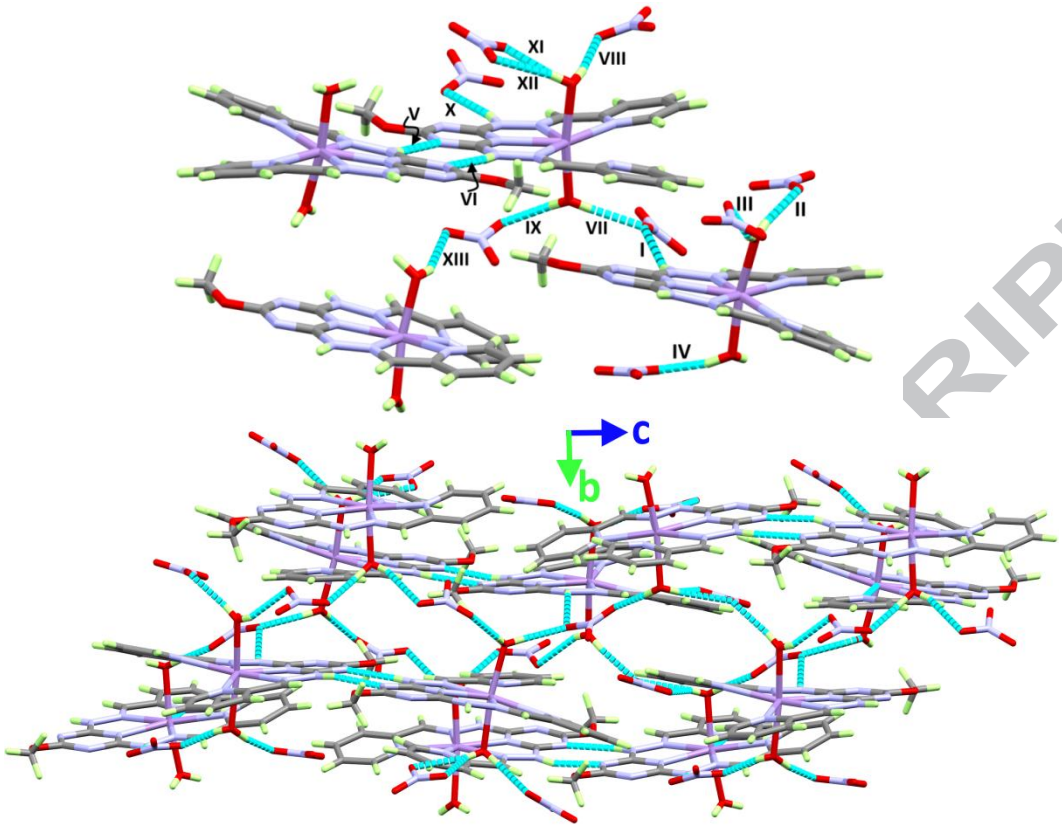

Fig. 5 The most important hydrogen bonding interactions; (**A**) (see **Table 5** for Latin numbering) and the three dimensional H-bonding network in the crystal structure of complex **7** (**B**).

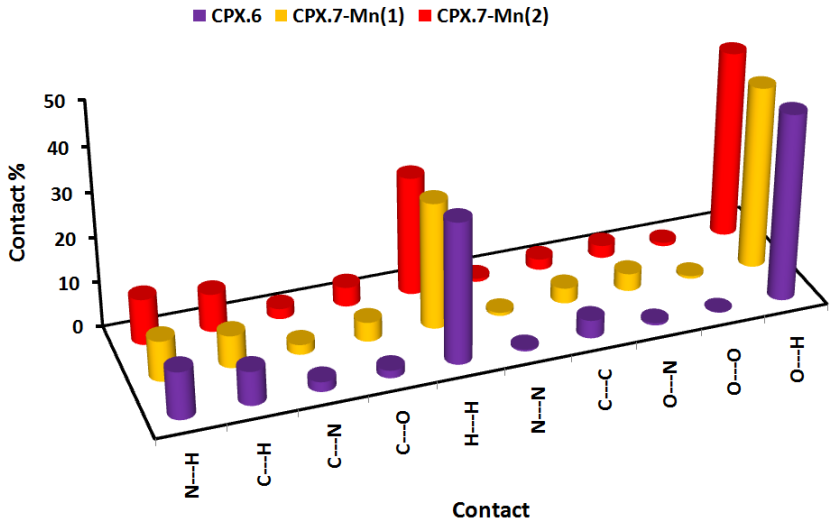

Fig. 6 Summary of the intermolecular interactions and their percentages in the crystal structure of the studied complexes.

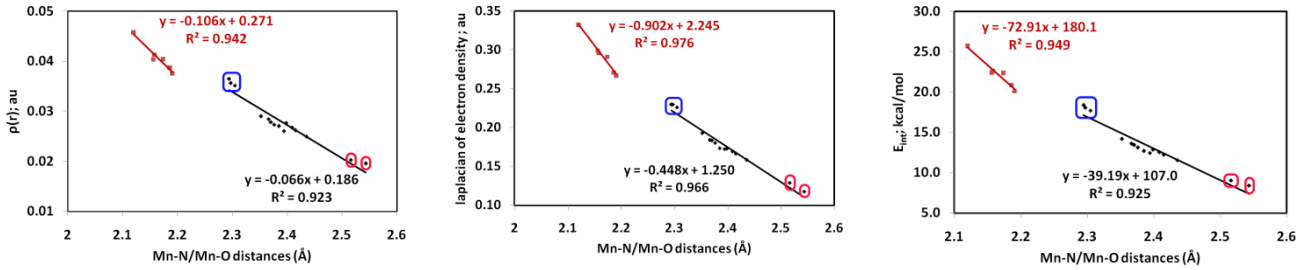

Fig. 7 Variation of electron density (ρ(r); a.u.), laplacian of electron density ($\nabla^2\rho(r)$; a.u.) and interaction energies ($E_{int.}$; kcal/mol) with the Mn-N and Mn-O distances (Å) at the corresponding bond critical point of these bonds. Note the low ρ(r), $\nabla^2\rho(r)$ and $E_{int.}$ at the BCPs of the two weak Mn-N(pyridine), indicated by red rectangle while the blue one for the strong Mn-N(triazine).

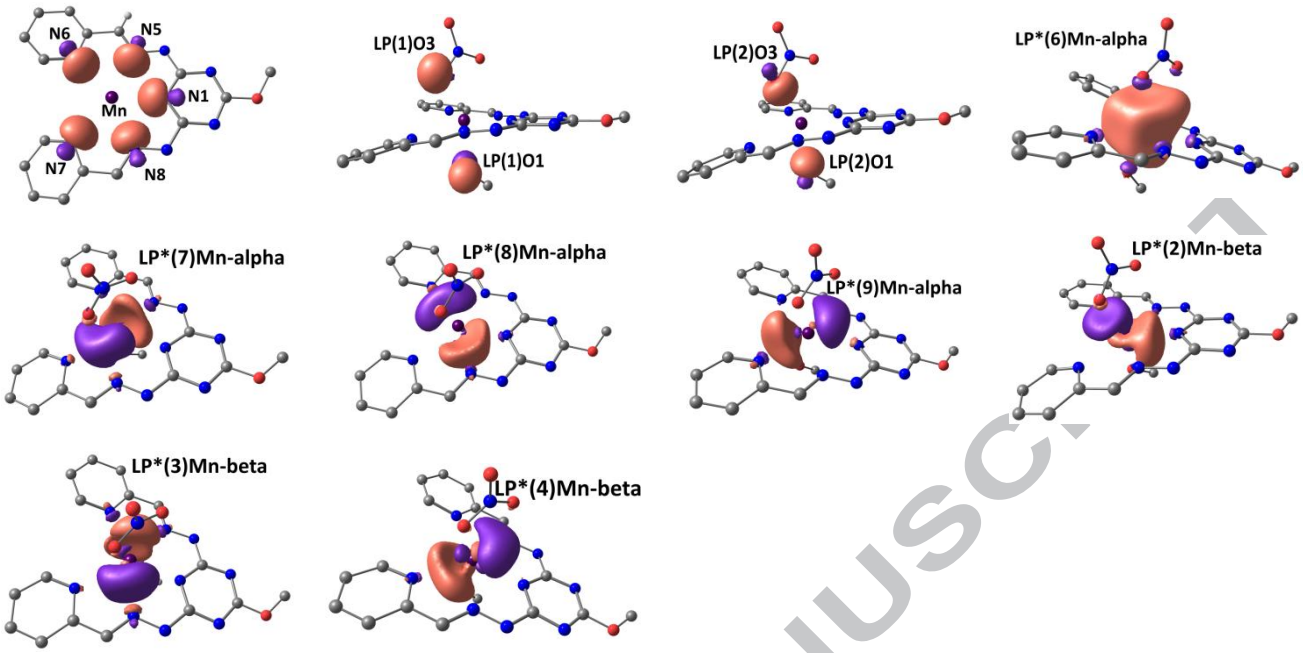

Fig. 8 The most important interacting natural orbitals shared in the Mn-N and Mn-O interactions calculated using WB97XD method.

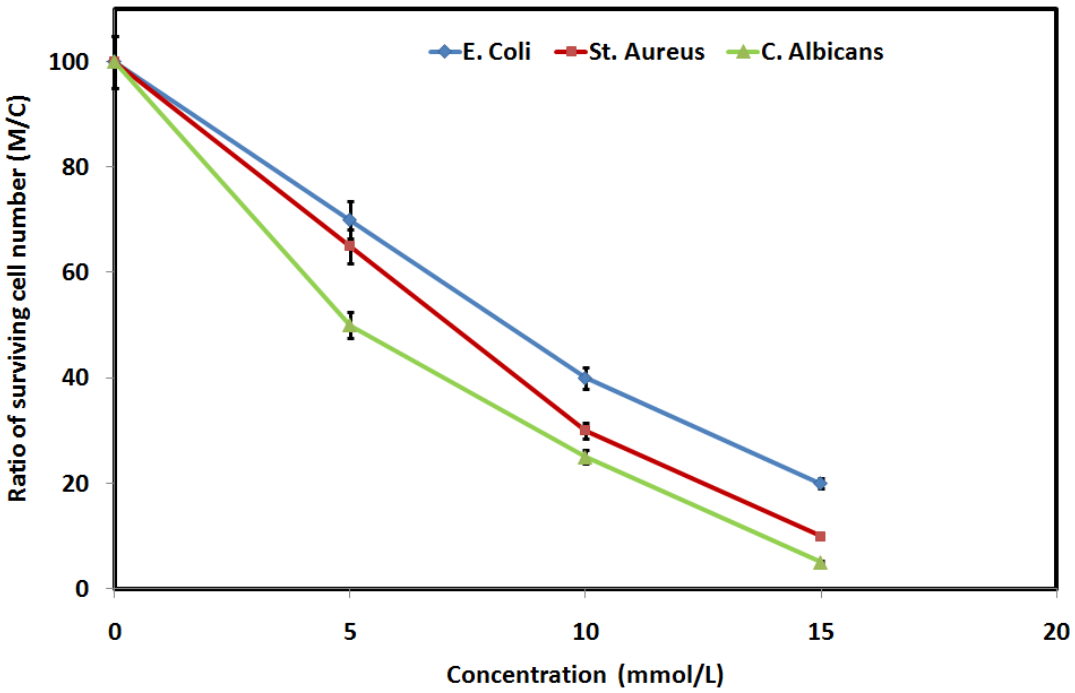

Fig. 9 Effect of concentration on growth and surviving cell number (M/C) for complex **7**.

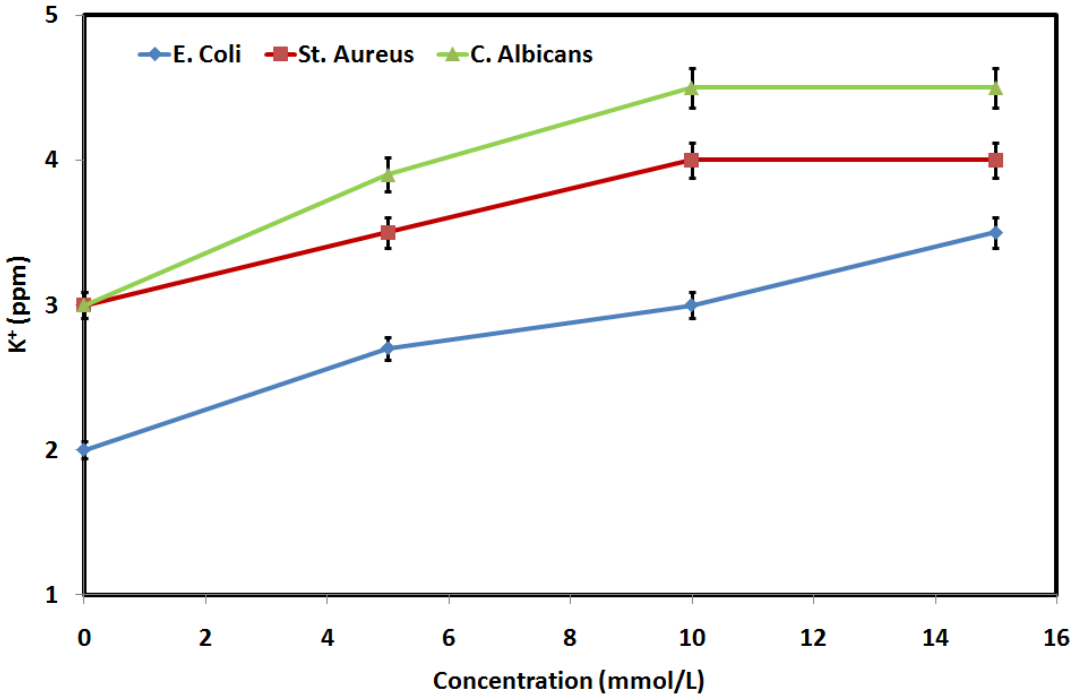

Fig. 10 Effect of concentration on K^+-ion flow for complex **7**.

Table 1 Crystal data and structure refinement for the studied complexes.

Compound	**Complex 6**	**Complex 7**
Empirical formula	$C_{18}H_{23}MnN_{11}O_9$	$C_{16}H_{19}MnN_{11}O_9$
Formula weight	592.41 g/mol	564.36 g/ mol
Temperature	115(2) K	293(2) K
Wavelength	0.71073 Å	0.71073 Å
Crystal system	Triclinic	Monoclinic
Space group	P-1	P121/n1
Unit cell dimensions	a=8.5678(7) Å	a = 16.343(17) Å
	b=9.9840(7) Å	b = 13.625(15) Å
	c=15.3599(12) Å	c = 21.86(2) Å
	α = 105.493(2)°	α = 90°
	β = 101.300(3)°	β = 108.867(16)°
	γ = 90.053(3)°	γ = 90°
Volume	1239.64(17) $Å^3$	4606.(9) $Å^3$
Z	2	8
Density (calculated)	1.587 g/cm^3	1.628 g/cm^3
Absorption coefficient	0.605 mm^{-1}	0.647 mm^{-1}
F(000)	610	2312
Crystal size	0.13 x 0.16 x 0.27 mm^3	0.11 x 0.28 x 0.31 mm^3
Theta range for data collection	2.20 to 25.35°	2.40 to 25.41°
Index ranges	-10<=h<=10, -12<=k<=12, -18<=l<=18	-19<=h<=19, -15<=k<=16, -26<=l<=26
Reflections collected	19875	41758
Independent reflections	4535 [R(int) = 0.0916]	8446 [R(int) = 0.0639]
Completeness to theta	99.9%	99.4%
Refinement method	Full-matrix least-squares on F^2	
Data / restraints / parameters	4535 / 0 / 366	8446 / 0 / 697
Goodness-of-fit on F^2	1.042	1.052
Final R indices [I>2sigma(I)]	R1 = 0.0423, wR2 = 0.0765	R1 = 0.0430, wR2 = 0.0976
R indices (all data)	R1 = 0.0741, wR2 = 0.0861	R1 = 0.0772, wR2 = 0.1149
Extinction coefficient	0.0018(5)	-
Largest diff. peak and hole ($e.Å^{-3}$)	0.309 and -0.353	0.504 and -0.352
CCDC	1815911	1815912

Table 2 Bond lengths (Å) and angles (°) for [MnL(MeOH)NO_3]NO_3.MeOH complex.

Mn1-O3	2.174(2)	Mn1-N8	2.385(2)
Mn1-O1	2.187(2)	Mn1-N6	2.398(2)
Mn1-N1	2.294(2)	Mn1-N7	2.544(2)
Mn1-N5	2.366(2)		
N1-Mn1-N5	65.84(8)	N8-Mn1-N6	160.92(7)
N1-Mn1-N8	65.82(8)	N1-Mn1-N7	130.71(8)
N5-Mn1-N8	131.43(8)	N5-Mn1-N7	157.69(7)
N1-Mn1-N6	133.00(8)	N8-Mn1-N7	66.01(7)
N5-Mn1-N6	67.64(7)	N6-Mn1-N7	95.88(7)
O3-Mn1-O1	154.48(7)		

Table 3 Hydrogen bonds [Å and °] for complex **6**.

No.	D—H···A	D—H (Å)	H···A (Å)	D···A (Å)	D—H···A (°)
I	O1-H1...O6	0.744(3)	1.979(3)	2.718(3)	171.9(3)°
II	O2-H2...O8	0.772(4)	2.027(4)	2.699(3)	145.4(4)
III	N4-H4A...O2^{i}	0.840(3)	1.924(3)	2.761(5)	175.2(3)
IV	N9-H9A...O6^{ii}	0.881(2)	1.991(2)	2.822(3)	157.0(2)

(i) x, 1+y,z; (ii) 1+x,y,z

Table 4 Bond lengths (Å) and angles (°) for $[MnL(H_2O)_2](NO_3)_2$ complex.

Mn1-O3	2.157(3)	Mn2-O5	2.120(3)
Mn1-O2	2.191(3)	Mn2-O6	2.158(3)
Mn1-N1	2.297(3)	Mn2-N10	2.305(3)
Mn1-N5	2.352(3)	Mn2-N14	2.370(3)
Mn1-N8	2.376(3)	Mn2-N17	2.394(3)
Mn1-N6	2.409(3)	Mn2-N15	2.436(3)
Mn1-N7	2.415(4)	Mn2-N16	2.516(4)
O3-Mn1-O2	171.07(11)	O5-Mn2-O6	170.81(10)
N1-Mn1-N5	66.20(9)	N10-Mn2-N14	65.78(9)
N1-Mn1-N8	65.49(11)	N10-Mn2-N17	65.34(11)
N5-Mn1-N8	131.69(9)	N14-Mn2-N17	131.10(9)
N5-Mn1-N7	159.82(9)	N17-Mn2-N15	160.47(9)
N8-Mn1-N7	67.23(11)	N14-Mn2-N15	67.31(9)
N1-Mn1-N6	132.73(11)	N10-Mn2-N15	132.73(11)

Table 5 Hydrogen bonds for the $[MnL(H_2O)_2](NO_3)_2$ complex; **7**.

No.	D—H···A	D—H (Å)	H···A (Å)	D···A (Å)	D—H···A (°)
I	N4-H4A…O11	0.860(3)	2.077(3)	2.832(4)	146.2(2)
II	O3-H3B…O15	0.774(5)	1.962(5)	2.726(5)	169.5(4)
III	O3-H3A…O16	0.680(5)	2.110(4)	2.745(6)	156.3(3)
IV	O2-H2B…O17^{i}	0.904(4)	1.926(4)	2.810(4)	165.6(4)
V	N9-H9A…N11^{ii}	0.860(3)	2.126(3)	2.960(4)	163.2(2)
VI	N18-H18…N2^{ii}	0.860(3)	2.128(3)	2.976(4)	168.6(2)
VII	O5-H5B…O11	0.781(4)	1.982(3)	2.757(4)	170.9(4)
VIII	O6-H6B…O12^{iii}	0.780(4)	2.082(2)	2.848(4)	167.5(4)
IX	O5-H5A…O7	0.725(3)	2.069(3)	2.784(4)	169.6(3)
X	N13-H14A…O7^{iv}	0.787(3)	2.252(3)	3.012(5)	162.7(2)
XI	O6-H6A… O14^{v}	0.779(4)	2.247(4)	2.870(4)	137.5(3)
XII	O6-H6A… O15^{v}	0.779(4)	2.252(4)	3.013(5)	165.7(3
XIII	O2-H2A…O8^{vi}	0.715(5)	2.296(5)	2.952(5)	153.4(3)

(i) 1.5-x,1/2+y,1.5-z; (ii) 1-x,1-y,1-z; (iii) 1/2-x,-1/2+y,1.5-z; (iv) -x,1-y,1-z; (v) -1/2+x,1/2-y,-1/2+z and (vi) -1/2+x,1.5-y,-1/2+z

Table 6 The net natural charges at Mn and ligand/anion fragments[a].

	CPX. 6	CPX. 7 (unit 1)	CPX. 7 (unit 2)
Mn	1.1562(1.1514)	1.1046(1.1011)	1.1218(1.1188)
L	0.4768(0.4739)	0.5362(0.5256)	0.5240(0.5154)
NO_3^-	-0.7874(-0.7821)[b]	-0.9637(-0.9578)[c]	-0.9692(-0.9646)[c]
NO_3^-	-0.9666(-0.9648)[c]	-0.9673(-0.9585)[c]	-0.9742(-0.9666)[c]
H_2O[d]		0.1263(0.1249)	0.1330(0.1315)
H_2O[e]		0.1639(0.1646)	0.1646(0.1655)
MeOH[b]	0.1200(0.1204)		
MeOH[c]	0.0010(0.0011)		

[a]Values inside and outside parentheses for the WB97XD and MPW1PW91
[b]coordinated [c]Ionic [d]weakly coordinated water [$H_2O(2)$ and $H_2O(6)$]
[e]strongly coordinated water [$H_2O(3)$ and $H_2O(5)$]

Table 7 Summary of the donor $NBO_{(i)}$→ acceptor $NBO_{(J)}$ interactions energies ($E^{(2)}$; kcal/mol) for the Mn-N and Mn-O interactions.

CPX. 6	**WB97XD**		**MPW1PW91**	
	Alpha(Beta)	Net	Alpha(Beta)	Net
LPO1→LP*Mn1	36.89(50.37)	87.26	33.53(42.77)	76.30
LPN1→LP*Mn1	33.59(42.62)	76.21	31.31(37.98)	69.29
LPN5→LP*Mn1	28.80(37.82)	66.62	25.99(30.64)	56.63
LPN6→LP*Mn1	27.79(35.54)	63.33	24.84(29.40)	54.24
LPN7→LP*Mn1	21.94(30.05)	51.99	19.48(24.73)	44.21
LPN8→LP*Mn1	29.01(35.04)	64.05	26.07(29.33)	55.40
LPO3→LP*Mn1	49.30(55.61)	104.91	48.50(57.12)	105.60
CPX.7 (unit 1)				
LPN1→LP*Mn1	35.81(45.84)	81.65	32.72(39.05)	71.77
LPN5→LP*Mn1	31.66(41.58)	73.24	28.18(35.17)	63.35
LPN6→LP*Mn1	28.63(38.15)	66.78	25.37(31.24)	56.61
LPN7→LP*Mn1	29.02(35.83)	64.85	25.85(28.99)	54.84
LPN8→LP*Mn1	38.61 (30.79)	69.58	27.99(32.38)	60.37
LPO2→LP*Mn1	35.96(51.14)	87.10	32.68(47.13)	79.81
LPO3→LP*Mn1	47.46(66.04)	113.50	43.07(56.82)	99.89
CPX.7 (unit 1)				
LPN10→LP*Mn2	35.68(44.88)	80.56	32.78(38.48)	71.26
LPN14→LP*Mn2	30.05(39.43)	69.48	27.27(32.46)	59.73
LPN15→LP*Mn2	26.60(35.97)	62.57	23.30(29.53)	52.83
LPN16→LP*Mn2	22.54(30.47)	53.01	19.69(24.75)	44.44
LPN17→LP*Mn2	28.77(36.53)	65.30	25.84(30.76)	56.60
LPO5→LP*Mn2	51.42(70.72)	122.14	46.49(60.32)	106.80
LPO6→LP*Mn2	37.31(51.79)	89.10	33.52(43.6)	77.12

Table 8 Diameters of inhibition zones (mm) of the tested compounds (15 mmol/L) against different species of microorganisms.

Microorganisms	Gen.[a]	L	CPX.6	CPX.7
E. coli	16.4	13.2	17.2	17.1
B. subtilus	17.4	9.8	20.6	17.0
K. pneumonia	17.4	14.4	17.8	18.3
St. aureus	19.4	11.8	17.5	16.9
S. typhimurium	18.4	10.2	15.0	15.2
C. albicans	13.9[b]	8.8	10.4	12.1

[a]Gen. = Gentamycin [b]fluconazole

Table 9 The MIC values (mmol/L) of the studied compounds against selected microorganisms.

Microorganism	L	CPX.6	CPX.7
E.coli	4.0	5.0	4.5
St.aureus	3.0	5.0	3.5
C.albicans	4.0	3.5	2.5

Highlights

- Two Mn(II) complexes (**6** and **7**) with giant *s*-triazine ligand (**L**) were synthesized.
- Complexes **6** and **7** have distorted pentagonal bipyramidal configuration around Mn(II).
- AIM topological parameters correlated well with the Mn-N distances.
- **L** and **7** are the best candidates as antifungal and antibacterial agents, respectively.
- Their reactivity depends on the interactions between the compound and cell wall

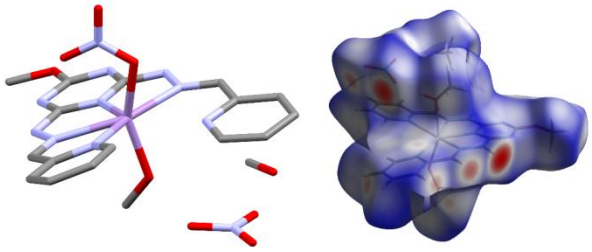

Complex 6

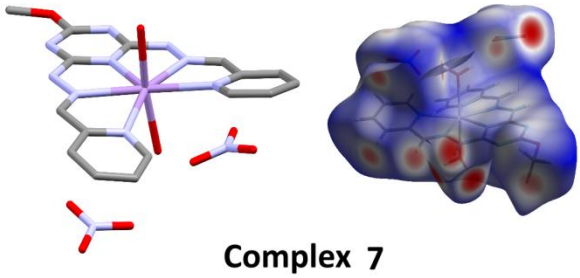

Complex 7